Predicting Maize Yield Using High-Resolution Imagery

Eli Baldwin

May 2019

A THESIS

Submitted to the faculty of Clark University,

Worcester, Massachusetts,

in partial fulfillment of

the requirements for

the degree of Bachelor of Arts

in the department of Geography

Abstract

Predicting Maize Yield Using High-Resolution Imagery

Eli Baldwin

The ability to predict crop yields during the growing season could be beneficial to a range of interested parties from individual farmers to policy makers to agricultural corporations. Methods have been developed to predict larger-scale, regional yields from remotely sensed imagery. In recent years, agricultural research has started focusing more on precision agriculture. I follow the method known as scalable crop yield mapping. This approach uses crop simulation models to find the relationship between vegetation indices and yield using regression. Then, the regression is applied to vegetation index images of fields, and the predicted yields are compared to actual yields to test the accuracy of the model. I use high-resolution UAS imagery, as well as calculate the relationship between vegetation indices and LAI based on field measurements. I did find within-field variation in the predicted yield images, although the R-squared values found in the regression are lower than those found by other authors and I did not have reliable measurements of actual yields. I relied on imagery from three fields which is inadequate, and a downside of using UAS imagery. It is usually much easier to obtain satellite images than UAS images.

Lyndon Estes, Ph. D.
Chief Instructor

John Rogan, Ph. D
Professor

Acknowledgements

My thesis advisor Professor Lyndon Estes and second reader Professor John Rogan. All my fellow students who were also involved in collecting and processing data that I used. Lei Song, Mike Cecil, Sitian Xe, Olivia Barksdale, Henrik Westerkam. The LEEP project grant that provided funding for my summer research. Professor Christopher Williams for lending the line quantum light sensor.

Table of Contents

List of Tables/graphs:

List of Maps/photographs

Introduction:

The ability to predict crop yields during the growing season could be beneficial to a range of interested parties from individual farmers to policy makers to agricultural corporations (Lobell, Thau, Seifert, Engle, & Little, 2015; Peralta, Assefa, Du, Barden, & Ciampitti, 2016; Schwalbert et al., 2018). The ability to establish a relationship between remotely sensed vegetation indices and the healthiness of crops is long established (Bu, Sharma, Denron, & Franzen, 2017; Du & Noguchi, 2017; Nebiker, Lack, Abächerli, & Läderach, 2016). In the past, remotely sensed imagery was used only at a larger scale. For example, assessing variation between different regions or even countries (Du & Noguchi, 2017; Lobell et al., 2015; Peralta et al., 2016; Schwalbert et al., 2018). This was due to a lack of adequate data and to the prioritization of large-scale agricultural studies. In recent years the focus of agricultural research and policy has shifted to precision agriculture (Peralta et al., 2016). This includes an emphasis on within-field variability as opposed to between field variability (Du & Noguchi, 2017; Nebiker et al., 2016; Peralta et al., 2016). Previous models of crop yield have tended to be site specific (Lobell et al., 2015; Peralta et al., 2016; Schwalbert et al., 2018). More recently, models have been developed with the goal of being applicable anywhere (Lobell et al., 2015; Peralta et al., 2016; Schwalbert et al., 2018)

The scalable yield crop mapper was introduced by Lobell et. al. in 2015. The scalable yield mapper uses regression to relate a vegetation index and weather measurements to yield values generated with a mechanistic crop model that is then validated using actual data on yields and vegetation indices. The idea of the SCYM is to yield a model that is widely and easily usable, and does not require field data. Once calibrated, Lobell et. al.'s model only requires satellite imagery and weather data that can be acquired for free, probably from a government

agency. However, calibrating the SCYM requires more effort and a different model must be calculated for each day. The vegetation index of a crop in the middle of July relates to yield differently than that same index in late August. The models are crop specific but are intentionally calibrated to work with different varieties of the same crop. The calibration process is done using a crop simulator such as the Agricultural Production Systems Simulator (APSIM) or the Decision Support System for Agrotechnology Transfer (DSSAT) (Lobell et al., 2015). Lobell et. al. used the Green Chlorophyll Vegetation Index and a vector of weather measurements including cumulative rainfall and solar radiation, in a linear regression (2015). Schwalbert et. al. took a slightly different approach to estimating field level variations in yield using remotely sensed imagery (2018). They used multiple vegetation indices and stepwise regression to determine their model and did not use any weather variables. They also did not use a crop simulation model, instead dividing their field imagery into two groups, one for training the regression, and the other for testing it. They found that the red-edge NDVI was the vegetation index most highly correlated to yield. Schwalbert et. al. also tested their satellite imagery for spatial dependence using the Moran's I statistic. They found that there was spatial autocorrelation in the vegetation index values in the satellite imagery, which indicates that one of the assumptions of linear regression, independence, was violated. The authors decided to use a form of regression that takes into account spatial relationships. This regression performed better than the other (2018). Peralta et. al. followed a similar approach (2016). When they tested their imagery for spatial dependence they found that only one field had no statistically significant spatial autocorrelation in either vegetation indices or actual yield. When the authors used a regression technique taking into account spatial relationships, the results were improved. They also tested a set of vegetation indices, and found that different indices were retained in the model

for different fields, but that the red-edge NDVI was the most commonly retained (Peralta et al., 2016).

Part of this thesis is calculating the relationship between VIs and LAI for the study area. All three of the previously mentioned studies use correlations between vegetation indices and the Leaf Area Index (LAI) found in the literature (Lobell et al., 2015; Peralta et al., 2016; Schwalbert et al., 2018). However, Kang et. al. did a meta-analysis of the relationship between vegetation indices and LAI found in the literature and discovered significant variations across space (2016). This calls into question how accurately SCYM can be when it is calibrated in one area and then used in another. This is one of the reasons why I have tried to find the relationship between the LAI and various vegetation indices, specifically in my study area.

This thesis contributes to the literature in part by using UAV imagery, which is much higher resolution than satellite imagery, in a SCYM. This can give farmers a more accurate and detailed idea of which parts of their fields are performing better or worse, and likely a more accurate idea of what their yields will be (Du & Noguchi, 2017; Nebiker et al., 2016). UAVs have become more commercially viable in recent years, as have light weight multi-spectral cameras that are made for monitoring agriculture (Du & Noguchi, 2017; Nebiker et al., 2016). The objective of this thesis is to create a SCYM using UAV imagery and to assess its effectiveness. I primarily follow Lobell et al.'s methods in creating the SCYM, using DSSAT to simulate crop yields and GCVI to predict yields, although I also test other VIs.

Study Area:

This research was conducted on three fields planted with maize owned and farmed by Whittier Farms in Sutton, MA. Sutton has a snowy, humid, warm summer climate according to

the Koppen-Geiger climate classification system (NOAA, 2007). Data was collected in the summer of 2018.

Figure 1: study area

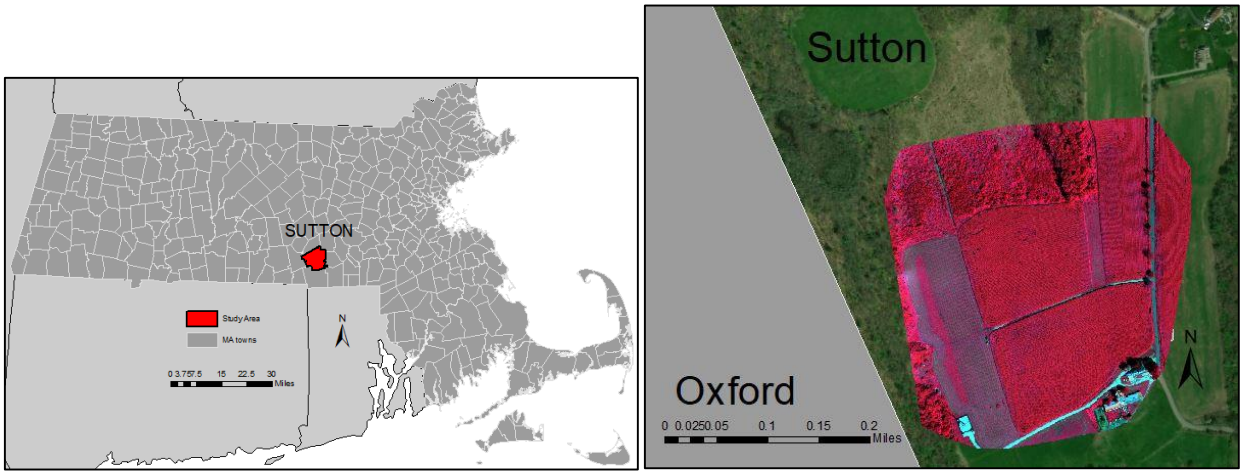

The position of Sutton within Massachusetts and a false color composite of the study area in Sutton, near the town border with Oxford.

Data:

We installed three Arable Mark sensors at the farm on the 8th of June. Arable Mark sensors are devices that are set above crop fields that take various agricultural and weather-related measurements and transmit them wirelessly to the user. The devices are referred to as upslope, midslope, and downslope. They took various measurements including sunshine, precipitation and growing degree days. The devices measure precipitation using a disdrometer, i.e. by acoustically sensing each raindrop that hits the top of the device. The study area was close enough to a pistol club shooting range that gunshots could be easily heard. We hypothesized that the gunshots caused the devices to record precipitation when there was none. I did notice very small amounts of precipitation, around 0.1cm recorded on some clear days. Every hour they report the amount of upwelling and downwelling radiation from 7 spectral bands from blue to near infrared (NIR). The devices calculate the (red-edge) normalized differential vegetation

index (NDVI) and the chlorophyll index (CI) daily. This data was accessed through the Arable website and the Arable R API. One of the devices stopped transmitting data for a few days, but when I took it down and restarted it, all the data was then available. Every device was taken down and the top was cleaned of dirt at least once over the summer.

Measurements of photosynthetically active radiation (PAR) were taken on twelve dates over the summer from June 21st to September 6th. These measurements were taken using a line quantum light sensor made specifically for measuring PAR underneath a canopy. Measurements were taken around every Arable Mark device. At each device there were four sets of measurements taken (see figure 2). The PAR meter was held diagonally away from the device so that it was underneath two rows of maize. Measurements were taken at (my) shoulder, waist, knee and ankle heights. Measurements were omitted if the maize was not yet tall enough to warrant them. Measurements of light above the canopy were also taken. These measurements were taken in the field until the maize grew too high and then they were taken just outside the field.

Figure 2, the author taking PAR measurements in the field

The UAV used in this study was and eBee plus drone made by SenseFly with the Parrot Sequoia multi-spectral sensor. There were five UAV flights total. The Sequoia camera has five sensors. One that captures regular digital images (RBG), one that captures green band images, one for red band images, red-edge band, and NIR. The images have approximately 11cm sided pixels. The overlap between images is at least 80%. However, there are more overlapping images towards the center of the flight area than at the edges, making the data closer to the center of the images better than the data near the edges. The farthest away from the center edge of the field designated as downslope was not captured because the UAV would have been too close to the neighboring property.

I also obtained data for use in DSSAT. This included soil data from the USGS and meteorological data from the NASA agrometeorological database. This includes data on temperatures and rainfall from 2010 to 2018.

Methods:

As mentioned previously red-edge NDVI and GCVI were calculated by the Arable Mark devices. One of the devices calculated GCVI values barely above zero for most of the season. This is clearly a mistake and those values were omitted. In the literature I found numerous VIs that were used to estimate LAI (Guindin-garcia et al., 2012; Kang et al., 2016; Viña, Gitelson, Nguy-Robertson, & Peng, 2011). NDVI (red-edge and red) and chlorophyll indices (CIs) were among the most commonly used, and best performing (Chang & Shoshany, 2016; Gitelson, Arkebauer, Rundquist, Keydan, & Leavitt, 2003; Viña et al., 2011). I decided to calculate three other VIs as well. The other most common, and commonly good VI is the Wide Dynamic Range VI (WDRVI) (Chang & Shoshany, 2016; Guindin-garcia et al., 2012). This was introduced by Gitelson for the express purpose of improving the estimation of LAI from NDVI because NDVI

has a tendency to saturate quickly in relation to the LAI (Gitelson, 2004). The WDRVI moderates the impact of the NIR band so the red band does not get overshadowed by it (Gitelson, 2004). The last two VIs that I calculated and tested are newer. The red-edge ratio NDVI includes the effects of the red-edge band, which is important to agriculture (Chang & Shoshany, 2016). The red-edge red CI adds the red edge band to the denominator and the variable a that can be any number from 0-1. If a is 0 this index is just the red CI. If a =1 than the red band is entirely replaced by the red-edge band. The values the creators suggest using are between 0.4 and 0.6, based on their tests of the index. The creators of this index suggests that it is more appropriate for estimating LAI and found that it had a higher R-squared than the traditional indices when regressed against LAI (Xie et al., 2018). The equations for these indices are as follows (figure 3):

Figure 3: VI equations

Red-edge NDVI	(NIR-RE)/(NIR+RE)
CI	(NIR/green)-1
WDRVI	(a*NIR-red)/(a*NIR+red)
Red-edge ratio NDVI	(NIR-red)/(NIR+red)*sqrt(RE)
Red-edge red CI	(NIR/(a*RE+(1-a)*red))-1

I calculated the values used for the bands in the equations by dividing the upwelling value for that band by its downwelling value, which yields reflectance values. The literature suggests that the a used to calculate WDRVI should be somewhere between 0.05 and 0.2 (Gitelson, 2004). The most common value used in the literature was 0.2 so that is what I used. The a in red-edge red CI should be somewhere between 0.4 and 0.6 according to the creators (Xie et al., 2018), so I chose 0.5. The LAI values come from Henrik Westerkam who calculated LAI from the measurements of PAR using the formula:

$$LAI = -2*\cos(Szen)*\ln(Qi/Qo)$$

Where Szen = solar zenith angle, Qi = PAR at ankle level, and Qo = PAR above the corn. The LAI values for each device are an average of all four PAR measurements taken around the device (H. Westerkam, personal communication, December 13th, 2018).

DSSAT requires a multitude of inputs, many of which can be estimated (Hoogenboom et al., 2017). The soil and weather data mentioned earlier were input into the model. The soil variables used in DSSAT include organic matter content, pH, oxygen and water content, mineral content, drainage rate and the sand, silt and clay content. The other main input to DSSAT is the cultivar. One of the main parts of the cultivar file that DSSAT requires are the P1 and P5 variables. P1 is the amount of Growing Degree Days (GDD) from emergence to silking. P5 is the amount of GDDs from silking to maturity (Hoogenboom et al., 2017). I took the values for GDDs from the Arable Mark sensors and my observations of maize emergence and silking as well as an estimate of maturity based on known characteristics of maize and the time of harvesting to determine these values. Then I varied the P1 and P5 values by ten to twenty more or fewer GDDs to create five total cultivars, as the scalable yield model is supposed to be generalizable to many varieties. Using the R implementation of DSSAT, thousands of simulations were created across nine years (2010-2018), the five cultivars, and three fields.

Each DSSAT simulation outputs daily LAI values and end of season yield values. In R studio, I combined these so that each observation was a DOY from one simulation which had an LAI value, the yield from that simulation, and an index value. I then added the weather variables maximum temperature and precipitation. From the precipitation data I calculated a cumulative precipitation for each date from the start of the year. These variables were chosen because they are thought to have an impact on agriculture production. I expect both of these variables to be positively correlated with yield. I calculated GCVI and red-edge NDVI values for each simulated

observation from the LAI using the regression equations I had previously established for them (see figure 6). I then used the linear model (lm) in R to evaluate the regression equation

$$Yield = \alpha + VegetationIndex_i * \beta + MaxTemp_i * \beta_1 + CumulativePrecip_i * \beta_2$$

for both vegetation indices for each day (i) between DOY 196 and 258, which is July 15th to September 15th on non-leap years. These dates were chosen because prior to the middle of July the explanatory power of the models is low and being able to predict the yield becomes less useful for the purpose of forecasting the yield in the future the closer the crop is to harvest.

I calculated the GCVI for each set of UAV images. Due to data and time constraints I did not manage to do the same for the red-edge NDVI. I then applied the regression equation found using the DSSAT simulated outputs to each pixel of the raster GCVI images, creating new raster images that had the yield predicted for each pixel. Unfortunately, Whittier Farms did not get an accurate estimation of the yield from the three fields in question, so I used an average of the yield simulated by DSSAT for 2018 for each field. I then calculated the Pearson's R correlation coefficient and root mean squared error (RMSE) for each date across all three fields, and the RMSE for each field on each date. I also produced predicted yield maps to assess the possibility of observation of within-field yield variations.

Results/Discussion:

LAI and VIs

The following (figure 4) are graphs showing the relationships between the five vegetation indices and LAI:

Figure 4: graphs of the relationships between each VI and LAI

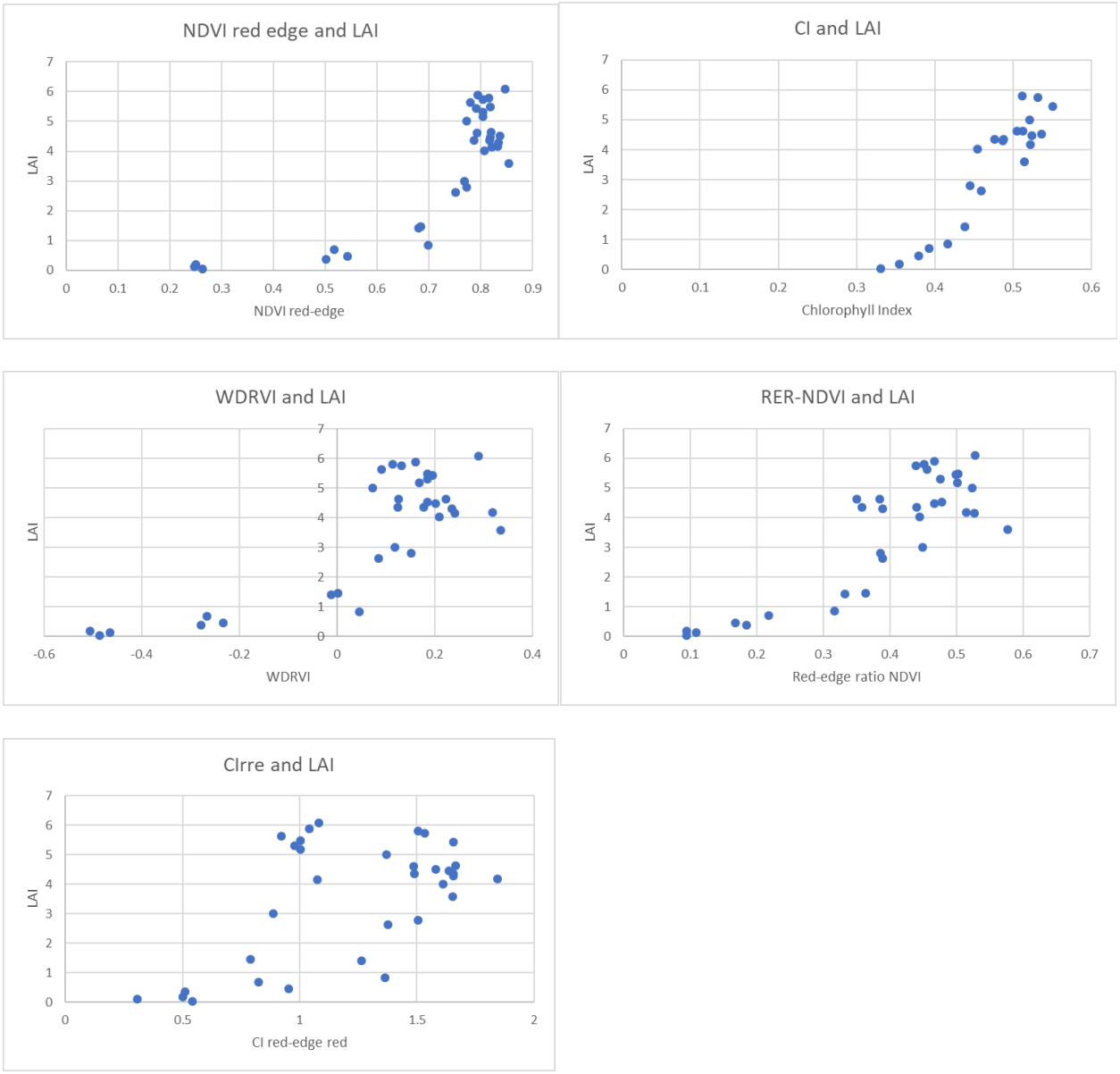

The graphs all appear to show exponential relationships. The CI however, has an almost linear relationship with LAI. The red-edge NDVI does seem to saturate at 0.8 as evidenced by the vertical cluster of dots. This is better than the literature suggests for the regular NDVI where saturation usually occurs at 0.7. The first two graphs appear to have strong relationships, the second two slightly weaker relationships, and the last graph has a much weaker relationship. The

red-edge red CI values calculated for the midslope device were noticeably and consistently lower than the values for the other two devices.

I ran the curve fitting module (within regression) in SPSS with LAI as the dependent variable and each index in turn as the independent variable. I selected both linear and exponential options. All the resulting exponential models were significant, and all had higher R-squared values than the linear regression except for CI. I also calculated the mean absolute error values for each vegetation index using the "mae" function in the "Metrics" R package. The following table (figure 5) contains R-squared and Mean Absolute Error (MAE) values for each of the indices:

Figure 5: VI and LAI relationship measures of fit

Index	Regression Type	R-squared	Mean Absolute Error
NDVI red-edge	exponential	0.923	0.758
CI	linear	0.870	0.573
WDRVI	exponential	0.863	1.21
RERndvi	exponential	0.832	1.29
CI red-edge red	exponential	0.488	5.00

The red-edge NDVI had the highest R-squared value. CI, WDRVI and red-edge ratio NDVI had reasonably high but lower R-squared values. The CI also has a lower MAE value than the NDVI. The red-edge red CI had a low R-squared and a high MAE. Due to the odd values that were calculated from the midslope device, I would guess that there was a problem with the device. However, the device's red-edge and red bands were used in the calculation of other indices and those measurements did not appear to be compromised. The red-edge ratio NDVI was originally calculated using Sentinal imagery(Xie et al., 2018), and there is a discrepancy in wavelengths used for red-edge bands between Sentinel and our sensors. Xie et al. report using a red edge band

from 680-750nm (2018), while the Arable mark devices red-edge band is 690-740. In addition, it is a relatively untested index and it is possible that the authors of the study introducing it just got lucky in having a higher R-squared value. The R-squared values I obtained are slightly smaller than most of the R-squared values I saw in the literature (Chang & Shoshany, 2016; Gitelson, 2004; Kang et al., 2016; Viña et al., 2011; Xie et al., 2018). This is possibly due to error in LAI measurements which were not calculated directly (which would involve measuring the surface area of every leaf in a given area).

This analysis seems to suggest the use of red-edge NDVI or CI to estimate LAI. However, the quick saturation of the NDVI is cause for concern, suggesting that the index with the second highest R-squared, the lowest MAE and a linear relationship to LAI, is likely the better candidate. One other study came to a similar conclusion and suggest that a piecewise regression should be used (Nguy-Robertson et al., 2012). This way an index that captures more of the variation in LAI at lower values can be used at lower values, and an index that captures more of the variation in LAI at higher values can be used at higher values. After their method I made a piecewise regression using red-edge NDVI until that index gets above 0.77 at which point the regression switches to CI. Using this method, the R-squared values are lower for the both steps, but especially the second one. However, the R-squared values of piecewise regressions are not interpretable. The resulting equations for the red-edge NDVI, CI and piecewise are as follows (figure 6):

Figure 6: equations to convert between VI and LAI

	1st step	2nd step
NDVI red-edge	$0.14e^{7.114x}$	N/A
CI	-10.004+28.411*x	N/A
piecewise	$0.18e^{6.353x}$	-1.491+12.036*x

Running DSSAT

All the models were found to be statistically significant as well as all the variables in every model, at the 99% confidence level (see appendix 1). The coefficients are all positive, as was expected. The graph below (figure 7) displays the R-squared values for the models using GCVI and red-edge NDVI.

Figure 7: graph of adjusted R-squared values by DOY

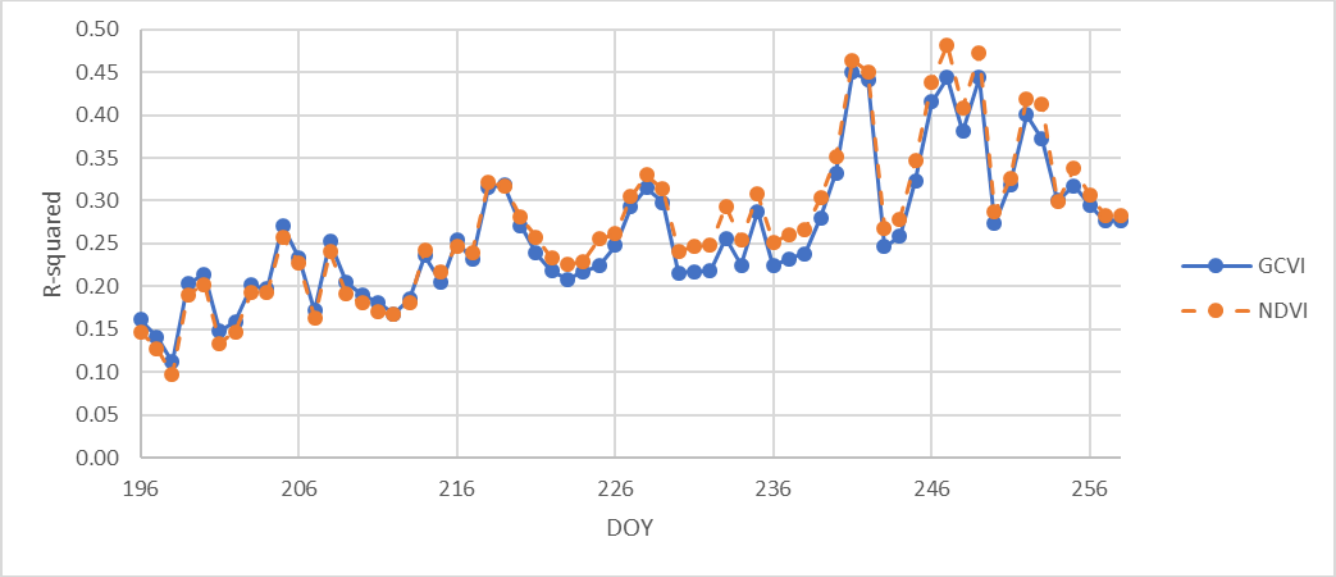

The R-squared values range from 0.1 to nearly 0.5. The mean of the R-squared values for the GCVI models is 0.26 and for the red-edge NDVI models, 0.27. This finding is in keeping with the earlier finding that red-edge NDVI is more highly correlated with LAI, which is known to be

correlated to yield, than GCVI. The models using GCVI performed slightly better earlier in the season, while the red-edge NDVI models performed better for most of the season. This is the opposite of what was expected, as the saturation of the red-edge NDVI index does not seem to have negatively impacted model performance, at least not relative to GCVI. The R-squared values generally increase later in the season, as was expected. However, the increase is not very linear. This could be a result of variations in the weather data input into DSSAT, which likely accounts for some of the variation between days. The highest R-squared values are between DOY 240-253, with a maximum of 0.48 on DOY 247. Even during this period there are R-squared values that are around the overall average. Lobell et al. found that the highest R-squared values were found between DOY 225-235, slightly earlier in the season. They also found R-squared values closer to 0.8, much higher than those found here (Lobell et al., 2015).

Correlation and RMSE:

Figure 9: correlation and RMSE

Date	correlation	RMSE
19-Jul	-0.072	4736.643
2-Aug	-0.13	1288.098
10-Aug	-0.878	909.899
24-Aug	-0.164	1147.11

The correlation values of simulated and predicted yield are all negative and quite erratic. I used correlation as that was the method used in the literature. That method did not work well here due to the lack of diversity in the yield values and the small number of fields. The RMSE term was more useful. The RMSE for the first date is high, indicating that the yield values produced from the raster images is not similar to the yield values produced by DSSAT. I did notice that the GCVI values in the imagery from July 19th were higher than those from the other images. This is anomalous as I would expect the GCVI to increase from mid-July to August, and

the Arable Mark devices show an increase in GCVI over that time period. This could be the result of an issue with the UAV or camera, or the result of a problem from image processing. The RMSE values for the other three dates are much lower, indicating that the pixel yield values are much more similar to the DSSAT yield values.

Figure 10: RMSE values for each field and date

Field	Date	RMSE
upslope	19-Jul	3787.198
upslope	2-Aug	1248.407
upslope	10-Aug	921.718
upslope	24-Aug	1482.78
midslope	19-Jul	5054.125
midslope	2-Aug	1020.244
midslope	10-Aug	881.286
midslope	24-Aug	1050.311
downslope	19-Jul	4904.915
downslope	2-Aug	1686.654
downslope	10-Aug	932.981
downslope	24-Aug	1014.728

All of the fields follow of the general pattern of having the highest RMSE on the first date and much lower RMSEs for the rest. If we ignore July 19th, then midslope has noticeable lower RMSEs for the other three dates combined and the absolute lowest RMSE at 881.286. There is no single way to determine how good an RMSE value is and no threshold because RMSE values are in the same units as the values they are evaluating. For context, most of the yield values were around 9000 to 10000. Lobell et al. only reported the correlation coefficients and not the RMSEs for their models, so direct comparisons are hard to make between my findings and theirs. They reported correlation coefficients of between 0.38 and 0.76.

I have displayed here the predicted yield maps for August 10th, because the predictions for that date have the lowest RMSE.

Figure 11: Predicted yield map for August 10th

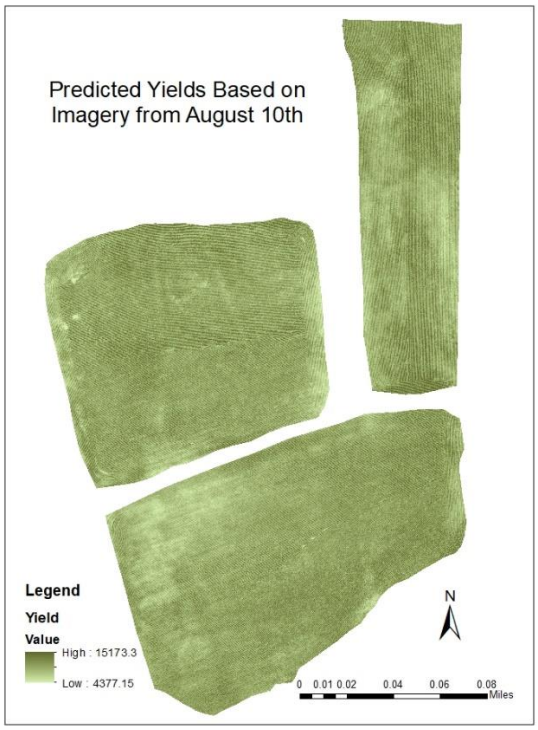

From this map (figure 11), one can see some areas of concern for the owner. The northwest corner of the southernmost field has noticeably lower values than the rest of the fields as well as some areas of the middle of the northeastern field. There are also three small areas in the northeastern part of the northeastern field that appear to be errors because of the homogeneity of low values that do not fit with the rest of the map where the values are patterned like one would expect a crop field to be.

Conclusion:

Although there have been many new vegetation indices created in recent years, the GCVI and the NDVI were still found to be the best. Using the red-edge band instead of the red band in the NDVI is a somewhat recent idea and I found it to be useful in an agricultural context as was

indicated by the literature. The concern that the red-edge NDVI would saturate was not borne out in this research. However, as the red-edge NDVI was not calculated for the UAV imagery and there being no predicted values to compare to simulated values this conclusion is tentative.

The adjusted R-squared values obtained using the regression of simulated yield and VIs (as well as weather data) were much smaller than what was found in the literature. In terms of future research this suggests that I need to go back and take another look at the inputs put into DSSAT. Also, I could consider trying to use relationships between VIs and LAI from the literature and comparing the results to those that I found. If I had been able to calculate the red-edge NDVI for all the images I could have used the VI that performed the best for each day for which I had imagery. For example, using the GCVI for July 19th, but the red-edge NDVI for August 10th.

This was a first attempt at replicating the scalable yield model using high resolution UAV imagery. This attempt yielded some insights into the limitations of this method. The small number of dates with imagery was a hindrance, especially when the imagery for one of those dates was problematic. Not having the actual yield value was, of course, not ideal. However, having the overall yield value for all three fields combined also would not have been ideal. Even having the actual yield for each field individually would not give much variation in the model. Lobell et al. used many fields over a large area which all had reliable estimates of actual yields (2015). In order to replicate their work, it would be necessary to have more fields, or to have yield values for sections of each field. Having said that, this method does show some promise, and the predicted yield images do show within-field variation. However, as I cannot compare the within-field variation from the predicted yield images to actual within-field yield variation, this conclusion is tentative.

One improvement to this research could be the calculation of the Moran's I statistic to test for spatial autocorrelation in the regression residuals. This is somewhat tricky because DSSAT does not have spatial components, and the residuals would have to be kriged to between the coordinates of the arable mark pods, which is imprecise and beyond the scope of this thesis. If there was statistically significant spatial autocorrelation, this would suggest that the methods suggested by (Schwalbert et al. 2018) and (Peralta et al. 2016) would likely be an improvement because of the use of regression techniques that take into account spatial relationships. However, those methods require even more imagery because half of it is used for training the regression, exacerbating the difficulty of obtaining enough UAS imagery.

Citations:

Bu, H., Sharma, L. K., Denron, A., & Franzen, D. W. (2017). Comparison of Satellite Imagery and Ground-Based Active Optical Sensors as Yield Predictors in Sugar Beet, Spring Wheat, Corn, and Sunfl ower. *Agronomy Journal*, *109*(1), 299–308. https://doi.org/10.2134/agronj2016.03.0150

Chang, J., & Shoshany, M. (2016). Red-Edge Ratio Normalized Vegetation Index for Remote Estimation of Green Biomass. *International Geoscience and Remote Sensing Symposium*, 1337–1339.

Du, M., & Noguchi, N. (2017). Monitoring of Wheat Growth Status and Mapping of Wheat Yield ' s within-Field Spatial Variations Using Color Images Acquired from UAV-camera System. *Remote Sensing*, *9*, 289–303. https://doi.org/10.3390/rs9030289

Gitelson, A. A. (2004). Wide Dynamic Range Vegetation Index for Remote Quantification of ... *Journal of Plant Physiology*, *161*(2), 165–173.

Gitelson, A. A., Arkebauer, T. J., Rundquist, D. C., Keydan, G., & Leavitt, B. (2003). Remote estimation of leaf area index and green leaf biomass in maize canopies. *Geophysical Research Letters*, *30*(5), 4–7. https://doi.org/10.1029/2002GL016450

Guindin-garcia, N., Arkebauer, T. J., Shanahan, J., Weiss, A., Guindin-garcia, N., Gitelson, A. A., … Weiss, A. (2012). An evaluation of MODIS 8- and 16-day composite products for monitoring maize green leaf area index monitoring maize green leaf area index. *Agricultural and Forest Meteorology*, *161*, 15–25. https://doi.org/10.1016/j.agrformet.2012.03.012

Kang, Y., Özdo, M., Zipper, S. C., Román, M. O., Walker, J., Young, S., … Alpilles, L. (2016). How Universal Is the Relationship between Remotely Sensed Vegetation Indices and Crop

Leaf Area Index ? A Global Assessment. *Remote Sensing*, *8*, S1–S23. https://doi.org/10.3390/rs8070597

Lobell, D. B., Thau, D., Seifert, C., Engle, E., & Little, B. (2015). Remote Sensing of Environment A scalable satellite-based crop yield mapper. *Remote Sensing of Environment*, *164*, 324–333. https://doi.org/10.1016/j.rse.2015.04.021

Nebiker, S., Lack, N., Abächerli, M., & Läderach, S. (2016). LIGHT-WEIGHT MULTISPECTRAL UAV SENSORS AND THEIR CAPABILITIES FOR PREDICTING GRAIN YIELD AND DETECTING PLANT DISEASES. *The International Archives of the Photogrammetry, Remote Sensing and Spatial Information Sciences*, *31*(B1), 12–19. https://doi.org/10.5194/isprsarchives-XLI-B1-963-2016

Nguy-robertson, A., Gitelson, A., Peng, Y., Viña, A., Arkebauer, T., & Rundquist, D. (2012). Green Leaf Area Index Estimation in Maize and Soybean: Combining Vegetation Indices to Achieve Maximal Sensitivity. *Agronomy Journal*, *104*(5), 1336–1347. https://doi.org/10.2134/agronj2012.0065

Peralta, N. R., Assefa, Y., Du, J., Barden, C. J., & Ciampitti, I. A. (2016). Mid-Season High-Resolution Satellite Imagery for Forecasting Site-Specific Corn Yield. *Remote Sensing*, *8*, 848–864. https://doi.org/10.3390/rs8100848

Schwalbert, R. A., Amado, T. J. C., Nieto, L., Varela, S., Corassa, G. M., Horbe, T. A. N., … Ciampitti, I. A. (2018). Forecasting maize yield at field scale based on high-resolution satellite imagery. *Biosystems Engineering*, *171*, 179–192. https://doi.org/10.1016/j.biosystemseng.2018.04.020

Viña, A., Gitelson, A. A., Nguy-robertson, A. L., & Peng, Y. (2011). Remote Sensing of Environment Comparison of different vegetation indices for the remote assessment of green

leaf area index of crops. *Remote Sensing of Environment*, *115*, 3468–3478. https://doi.org/10.1016/j.rse.2011.08.010

Xie, Q., Dash, J., Huang, W., Peng, D., Qin, Q., & Mortimer, H. (2018). Vegetation indices combining the red and red-edge spectral information for leaf area index retrieval. *IEEE Journal of Selected Topics in Applied Earth Observations and Remote Sensing*, *11*(5), 1482–1493.

Appendix: regression coefficients and test statistics

NDVI	Estimate	Std. Error	t value	Pr(>|t|)
(Intercept)	-2115.64	311.6591	-6.78831	1.14E-11
NDVI	32509.47	381.0908	85.30637	0
T2M_MAX	-442.671	6.703365	-66.0371	0
Precip_cumsum	1.555316	0.041227	37.72538	3.35E-308
(Intercept)1	-8959.65	296.918	-30.1755	1.08E-198
NDVI1	32624.68	399.1261	81.74027	0
T2M_MAX1	-212.556	4.026576	-52.7883	0
Precip_cumsum1	1.414372	0.041308	34.23942	1.01E-254
(Intercept)2	-12059	332.1427	-36.3066	7.78E-286
NDVI2	32255.69	409.6921	78.73154	0
T2M_MAX2	-103.316	5.926839	-17.4318	6.69E-68
Precip_cumsum2	0.846461	0.041153	20.56862	1.02E-93
(Intercept)3	-26185	303.1682	-86.3713	0
NDVI3	31817.91	384.6527	82.71854	0
T2M_MAX3	374.2886	4.38713	85.31512	0
Precip_cumsum3	2.331138	0.041942	55.58034	0
(Intercept)4	-32836.7	329.9437	-99.5222	0
NDVI4	39918.8	385.5439	103.5389	0
T2M_MAX4	389.2705	4.429636	87.87865	0
Precip_cumsum4	2.068778	0.040706	50.82255	0
(Intercept)5	-23480.8	333.1377	-70.4838	0
NDVI5	36373.59	407.2672	89.31138	0
T2M_MAX5	168.6494	6.591161	25.58721	1.04E-143
Precip_cumsum5	0.941925	0.040087	23.49687	1.37E-121

(Intercept)6	-23581.6	319.049	-73.9121	0
NDVI6	38845.01	388.8903	99.88679	0
T2M_MAX6	105.3658	5.288576	19.92329	4.61E-88
Precip_cumsum6	1.027762	0.041424	24.81064	2.82E-135
(Intercept)7	-32917.3	341.8786	-96.2837	0
NDVI7	43642.21	369.9401	117.971	0
T2M_MAX7	294.7579	5.561144	53.00311	0
Precip_cumsum7	1.213292	0.039464	30.744	4.04E-206
(Intercept)8	-30629.9	322.6718	-94.9259	0
NDVI8	44338.4	365.0159	121.4698	0
T2M_MAX8	198.4836	4.05688	48.92519	0
Precip_cumsum8	0.763934	0.038591	19.79567	5.76E-87
(Intercept)9	-7231.08	287.0941	-25.1871	2.48E-139
NDVI9	31331.31	350.2891	89.44415	0
T2M_MAX9	-295.954	2.950809	-100.296	0
Precip_cumsum9	0.954613	0.037137	25.70517	5.20E-145
(Intercept)10	-7939.77	294.1714	-26.9903	1.38E-159
NDVI10	29591.86	355.7206	83.18849	0
T2M_MAX10	-234.285	2.834064	-82.6674	0
Precip_cumsum10	0.786504	0.037588	20.92423	6.60E-97
(Intercept)11	-12966.9	396.4172	-32.7101	7.77E-233
NDVI11	32587.43	398.8663	81.70014	0
T2M_MAX11	-123.536	5.4818	-22.5357	4.86E-112
Precip_cumsum11	0.470167	0.038886	12.09092	1.28E-33
(Intercept)12	1941.888	319.3822	6.080138	1.21E-09
NDVI12	23833.87	334.191	71.31811	0
T2M_MAX12	-417.403	4.593451	-90.8691	0
Precip_cumsum12	0.795381	0.037033	21.47781	5.56E-102
(Intercept)13	3542.627	376.6895	9.404634	5.38E-21
NDVI13	20874.83	350.8681	59.4948	0
T2M_MAX13	-382.363	5.851711	-65.3421	0
Precip_cumsum13	0.131747	0.038434	3.427864	0.000609
(Intercept)14	-4960.36	297.3947	-16.6794	2.48E-62
NDVI14	24585.39	322.0016	76.35175	0
T2M_MAX14	-198.006	3.719208	-53.2387	0
Precip_cumsum14	0.40837	0.03853	10.59862	3.17E-26
(Intercept)15	-5153.88	341.3245	-15.0996	1.98E-51
NDVI15	26998.21	303.4465	88.97188	0
T2M_MAX15	-262.291	7.002065	-37.4591	6.09E-304

Precip_cumsum15	0.600598	0.038648	15.54037	2.30E-54
(Intercept)16	-22495.3	419.1984	-53.6627	0
NDVI16	35068.5	330.9681	105.9573	0
T2M_MAX16	141.4319	8.363551	16.91051	5.12E-64
Precip_cumsum16	0.508908	0.038838	13.10337	3.52E-39
(Intercept)17	-15986	271.0164	-58.9855	0
NDVI17	33859.31	289.4051	116.9963	0
T2M_MAX17	-56.1234	6.636899	-8.45627	2.82E-17
Precip_cumsum17	0.567846	0.038411	14.78338	2.24E-49
(Intercept)18	-11368.7	229.5457	-49.5268	0
NDVI18	38315.36	281.7364	135.9972	0
T2M_MAX18	-354.541	5.139871	-68.9786	0
Precip_cumsum18	1.516877	0.039522	38.38054	8.31e-319
(Intercept)19	-15987.4	220.4094	-72.5349	0
NDVI19	39241.13	296.8564	132.1889	0
T2M_MAX19	-205.847	4.85597	-42.3904	0
Precip_cumsum19	0.808647	0.038215	21.16051	4.67E-99
(Intercept)20	-30716	281.649	-109.058	0
NDVI20	39896.26	281.9752	141.4885	0
T2M_MAX20	289.8943	4.947573	58.59323	0
Precip_cumsum20	1.269438	0.039265	32.3304	1.50E-227
(Intercept)21	-12396.7	261.4616	-47.4131	0
NDVI21	34349.91	283.8974	120.9941	0
T2M_MAX21	-196.527	3.94749	-49.7852	0
Precip_cumsum21	0.723433	0.037436	19.3243	5.65E-83
(Intercept)22	-1697.46	263.8416	-6.43365	1.25E-10
NDVI22	29013.51	274.4978	105.6967	0
T2M_MAX22	-442.401	4.160233	-106.34	0
Precip_cumsum22	2.125971	0.038331	55.46404	0
(Intercept)23	2180.349	290.8218	7.4972	6.60E-14
NDVI23	26451.35	282.1441	93.75121	0
T2M_MAX23	-522.97	4.999075	-104.613	0
Precip_cumsum23	2.404443	0.039397	61.03066	0
(Intercept)24	-2996.2	291.5679	-10.2762	9.42E-25
NDVI24	31172.04	279.9568	111.3459	0
T2M_MAX24	-452.873	5.516241	-82.0982	0
Precip_cumsum24	1.698881	0.038596	44.01722	0
(Intercept)25	-8025.86	279.1714	-28.7489	1.18E-180
NDVI25	31782.76	282.2167	112.6183	0

T2M_MAX25	-287.138	4.60718	-62.324	0
Precip_cumsum25	0.809774	0.036717	22.0546	2.09E-107
(Intercept)26	-7730.29	331.0056	-23.354	3.81E-120
NDVI26	30622.1	289.6525	105.7201	0
T2M_MAX26	-251.56	5.945494	-42.3111	0
Precip_cumsum26	0.604165	0.037234	16.22615	4.27E-59
(Intercept)27	-21668.7	243.0233	-89.1629	0
NDVI27	35054.86	263.0984	133.2386	0
T2M_MAX27	113.6365	4.942854	22.99005	1.66E-116
Precip_cumsum27	0.995469	0.040322	24.68778	5.77E-134
(Intercept)28	-14407.2	341.9353	-42.1342	0
NDVI28	32658.93	306.5658	106.5316	0
T2M_MAX28	-87.5057	5.781368	-15.1358	1.15E-51
Precip_cumsum28	0.622919	0.036873	16.8935	6.82E-64
(Intercept)29	-30122.5	309.7936	-97.2341	0
NDVI29	42521.37	296.3696	143.4741	0
T2M_MAX29	218.6683	4.659806	46.92648	0
Precip_cumsum29	0.940436	0.03716	25.30777	1.21E-140
(Intercept)30	-8435.06	273.4621	-30.8454	1.85E-207
NDVI30	28492.06	279.2387	102.0348	0
T2M_MAX30	-191.13	3.800965	-50.2845	0
Precip_cumsum30	0.54767	0.035712	15.33557	5.45E-53
(Intercept)31	-3838.44	251.4576	-15.2648	1.61E-52
NDVI31	25905.31	259.5542	99.80691	0
T2M_MAX31	-293.359	3.63516	-80.7004	0
Precip_cumsum31	1.015259	0.035184	28.85608	5.58E-182
(Intercept)32	-1778.79	240.2377	-7.40429	1.33E-13
NDVI32	27078.91	239.3386	113.1406	0
T2M_MAX32	-392.458	4.129829	-95.03	0
Precip_cumsum32	1.202683	0.034733	34.62686	2.03E-260
(Intercept)33	1483.316	280.0886	5.295882	1.19E-07
NDVI33	25293.6	248.4078	101.8229	0
T2M_MAX33	-439.984	5.145229	-85.513	0
Precip_cumsum33	0.786162	0.034529	22.76842	2.57E-114
(Intercept)34	-14088.7	260.7048	-54.0408	0
NDVI34	32085.89	250.4539	128.1109	0
T2M_MAX34	-75.9183	4.721911	-16.0779	4.69E-58
Precip_cumsum34	0.519785	0.036135	14.3845	7.61E-47
(Intercept)35	-21286.9	273.9107	-77.7147	0

NDVI35	35270.14	255.9563	137.7975	0
T2M_MAX35	96.06704	4.566663	21.0366	6.31E-98
Precip_cumsum35	0.913217	0.039608	23.05655	3.63E-117
(Intercept)36	-20012.8	260.7658	-76.7461	0
NDVI36	33909.52	239.1678	141.7813	0
T2M_MAX36	89.79619	5.064101	17.73191	3.44E-70
Precip_cumsum36	0.805597	0.038837	20.74326	2.82E-95
(Intercept)37	-30104.9	266.2708	-113.061	0
NDVI37	34075.42	219.4696	155.2626	0
T2M_MAX37	449.0999	6.807217	65.97409	0
Precip_cumsum37	1.418381	0.03723	38.09747	3.33e-314
(Intercept)38	-17879.9	199.1672	-89.7733	0
NDVI38	31787.75	219.3586	144.9122	0
T2M_MAX38	80.44829	4.555633	17.65908	1.25E-69
Precip_cumsum38	0.441099	0.035508	12.42266	2.15E-35
(Intercept)39	-22079.5	178.5149	-123.684	0
NDVI39	27746.75	216.9419	127.8995	0
T2M_MAX39	372.5726	5.059416	73.63944	0
Precip_cumsum39	0.933418	0.034982	26.68286	4.90E-156
(Intercept)40	-15469.1	190.3142	-81.2817	0
NDVI40	31823.91	223.5834	142.3357	0
T2M_MAX40	-10.0688	5.459046	-1.84442	0.065127
Precip_cumsum40	0.435353	0.035954	12.10854	1.03E-33
(Intercept)41	-18202.2	191.7774	-94.9133	0
NDVI41	31318.57	214.1862	146.2213	0
T2M_MAX41	102.6101	4.098842	25.03394	1.13E-137
Precip_cumsum41	0.510235	0.035687	14.2974	2.66E-46
(Intercept)42	-8609.24	248.7931	-34.604	4.41E-260
NDVI42	32010.87	212.2232	150.8359	0
T2M_MAX42	-261.283	7.396816	-35.3237	8.01E-271
Precip_cumsum42	0.484987	0.03542	13.69261	1.28E-42
(Intercept)43	-6168.4	202.9961	-30.3868	1.94E-201
NDVI43	30397.71	205.6512	147.812	0
T2M_MAX43	-304.272	4.45324	-68.326	0
Precip_cumsum43	0.824528	0.034896	23.6282	6.32E-123
(Intercept)44	165.8825	213.8835	0.775574	0.438003
NDVI44	25442.46	205.2329	123.9687	0
T2M_MAX44	-404.412	4.11067	-98.381	0
Precip_cumsum44	1.695233	0.034984	48.45717	0

(Intercept)45	5534.597	184.7246	29.96134	6.23E-196
NDVI45	18493.15	194.0655	95.29334	0
T2M_MAX45	-426.456	2.683678	-158.907	0
Precip_cumsum45	2.557071	0.032606	78.42249	0
(Intercept)46	10079.84	211.4637	47.66702	0
NDVI46	18521.69	195.3567	94.80961	0
T2M_MAX46	-574.768	3.817025	-150.58	0
Precip_cumsum46	1.712431	0.031554	54.26983	0
(Intercept)47	-16516.2	248.8716	-66.3643	0
NDVI47	31298.16	217.3813	143.9782	0
T2M_MAX47	46.02002	4.804983	9.577561	1.03E-21
Precip_cumsum47	0.788591	0.038593	20.43327	1.62E-92
(Intercept)48	-10556.7	199.9969	-52.7843	0
NDVI48	28596.71	207.2734	137.9662	0
T2M_MAX48	-88.5734	3.172728	-27.9171	1.58E-170
Precip_cumsum48	0.529524	0.035665	14.84723	8.70E-50
(Intercept)49	-3854.85	180.6115	-21.3433	9.77E-101
NDVI49	26589.77	190.4778	139.5951	0
T2M_MAX49	-272.599	3.125475	-87.2185	0
Precip_cumsum49	0.735558	0.033778	21.77595	9.08E-105
(Intercept)50	184.0787	161.8743	1.137171	0.255471
NDVI50	24950.63	175.5669	142.1147	0
T2M_MAX50	-394.166	2.812216	-140.162	0
Precip_cumsum50	2.395738	0.033709	71.07103	0
(Intercept)51	1659.761	151.9183	10.92535	9.20E-28
NDVI51	39287.82	173.3396	226.6523	0
T2M_MAX51	-853.047	5.229646	-163.118	0
Precip_cumsum51	3.758	0.035639	105.4464	0
(Intercept)52	-7127.78	134.8815	-52.8447	0
NDVI52	35349.37	178.5411	197.9901	0
T2M_MAX52	-410.486	3.375823	-121.596	0
Precip_cumsum52	2.317892	0.034877	66.45823	0
(Intercept)53	-4732.22	127.0955	-37.2335	2.35E-300
NDVI53	28723.79	159.052	180.5937	0
T2M_MAX53	-339.687	2.183554	-155.566	0
Precip_cumsum53	2.49427	0.032449	76.86631	0
(Intercept)54	-9294.65	204.303	-45.4944	0
NDVI54	26591.98	195.7064	135.8769	0
T2M_MAX54	-82.2867	3.95271	-20.8178	6.02E-96

Precip_cumsum54	0.671613	0.036597	18.35147	4.91E-75
(Intercept)55	-22028.8	195.6348	-112.602	0
NDVI55	33187.27	194.1429	170.9425	0
T2M_MAX55	215.3	3.297452	65.29284	0
Precip_cumsum55	1.901869	0.037655	50.50808	0
(Intercept)56	-28139.9	173.0522	-162.609	0
NDVI56	36816.88	177.9034	206.9487	0
T2M_MAX56	356.8518	2.846922	125.3465	0
Precip_cumsum56	2.855021	0.035405	80.63854	0
(Intercept)57	-27047	169.2159	-159.837	0
NDVI57	34972.99	172.5477	202.6859	0
T2M_MAX57	377.5572	3.086988	122.306	0
Precip_cumsum57	2.817768	0.035645	79.0512	0
(Intercept)58	-7416.04	165.3879	-44.8403	0
NDVI58	25954.71	176.1822	147.3174	0
T2M_MAX58	-132.569	3.33344	-39.7693	0
Precip_cumsum58	0.82973	0.034516	24.03877	3.80E-127
(Intercept)59	-18487.6	152.3616	-121.34	0
NDVI59	26265.9	166.2368	158.0029	0
T2M_MAX59	301.4226	4.028595	74.82077	0
Precip_cumsum59	0.946754	0.033352	28.38693	3.27E-176
(Intercept)60	-16616.8	163.7193	-101.496	0
NDVI60	26226.43	169.3933	154.8256	0
T2M_MAX60	232.7381	4.822119	48.2647	0
Precip_cumsum60	0.418087	0.03442	12.14647	6.50E-34
(Intercept)61	-12144.2	163.3977	-74.3231	0
NDVI61	26431.72	170.0259	155.457	0
T2M_MAX61	44.63002	4.014549	11.11707	1.10E-28
Precip_cumsum61	0.668477	0.034976	19.1127	3.26E-81
(Intercept)62	-12261.7	167.7637	-73.0891	0
NDVI62	26305.54	170.9871	153.8452	0
T2M_MAX62	53.07929	3.594959	14.76492	2.95E-49
Precip_cumsum62	0.677774	0.034911	19.4142	9.96E-84

GCVI	Estimate	Std. Error	t value	Pr(>|t|)
(Intercept)	15187.59	196.1867	77.41398	0
GCVI2	1414.406	15.32031	92.32226	0
T2M_MAX	-445.206	6.643321	-67.0155	0

Precip_cumsum	1.540073	0.040879	37.67404	2.23E-307
(Intercept)1	8417.046	131.0206	64.24214	0
GCVI21	1356.428	15.29641	88.67623	0
T2M_MAX1	-206.906	3.984675	-51.9254	0
Precip_cumsum1	1.414293	0.040966	34.52357	6.80E-259
(Intercept)2	5318.2	184.4191	28.83757	9.46E-182
GCVI22	1294.823	15.02741	86.16409	0
T2M_MAX2	-98.1282	5.870863	-16.7144	1.38E-62
Precip_cumsum2	0.869952	0.040761	21.34253	9.93E-101
(Intercept)3	-8620.19	142.6216	-60.441	0
GCVI23	1224.67	13.6521	89.7056	0
T2M_MAX3	372.5465	4.352018	85.60317	0
Precip_cumsum3	2.350046	0.041557	56.54977	0
(Intercept)4	-10239.4	154.7948	-66.148	0
GCVI24	1436.784	13.17017	109.0938	0
T2M_MAX4	383.2027	4.383782	87.41372	0
Precip_cumsum4	2.089387	0.040389	51.7311	0
(Intercept)5	-2796.24	192.4929	-14.5265	9.74E-48
GCVI25	1278.332	13.28653	96.21256	0
T2M_MAX5	164.3918	6.534272	25.1584	5.08E-139
Precip_cumsum5	0.967975	0.039695	24.38513	9.19E-131
(Intercept)6	-1152.73	161.0387	-7.15809	8.26E-13
GCVI26	1303.745	12.36731	105.4187	0
T2M_MAX6	98.5448	5.252551	18.76132	2.49E-78
Precip_cumsum6	1.055871	0.041069	25.70944	4.66E-145
(Intercept)7	-7087.79	180.4156	-39.2859	0
GCVI27	1398.697	11.51356	121.4825	0
T2M_MAX7	276.1085	5.506239	50.14467	0
Precip_cumsum7	1.257972	0.039235	32.06241	7.40E-224
(Intercept)8	-4061.94	141.3715	-28.7323	1.89E-180
GCVI28	1379.124	11.19048	123.2407	0
T2M_MAX8	174.6937	3.998454	43.69032	0
Precip_cumsum8	0.826103	0.038438	21.49192	4.11E-102
(Intercept)9	11063.32	102.9051	107.51	0
GCVI29	1006.601	10.35213	97.23612	0
T2M_MAX9	-302.462	2.904691	-104.129	0
Precip_cumsum9	0.992069	0.036663	27.05894	2.20E-160
(Intercept)10	9380.093	103.4279	90.69205	0
GCVI210	911.336	10.51174	86.69697	0

T2M_MAX10	-234.925	2.813733	-83.4922	0
Precip_cumsum10	0.835112	0.037322	22.37575	1.73E-110
(Intercept)11	6968.078	178.9575	38.93705	0
GCVI211	977.1903	11.33107	86.23987	0
T2M_MAX11	-151.355	5.237501	-28.8984	1.67E-182
Precip_cumsum11	0.510557	0.038639	13.21357	8.22E-40
(Intercept)12	16007.28	150.0314	106.6928	0
GCVI212	765.8008	9.677519	79.13193	0
T2M_MAX12	-429.191	4.463879	-96.1476	0
Precip_cumsum12	0.828715	0.036576	22.65713	3.17E-113
(Intercept)13	16113.62	189.3841	85.08436	0
GCVI213	678.1132	9.880413	68.63206	0
T2M_MAX13	-403.053	5.521557	-72.9962	0
Precip_cumsum13	0.128122	0.038104	3.362424	0.000773
(Intercept)14	9727.625	126.9545	76.62295	0
GCVI214	768.2187	9.367978	82.00474	0
T2M_MAX14	-214.166	3.597954	-59.5244	0
Precip_cumsum14	0.442467	0.038227	11.57463	5.93E-31
(Intercept)15	11666.74	203.2832	57.39158	0
GCVI215	843.5867	8.934423	94.41983	0
T2M_MAX15	-306.616	6.791296	-45.1484	0
Precip_cumsum15	0.664281	0.038259	17.36269	2.22E-67
(Intercept)16	678.1341	256.5023	2.643774	0.008201
GCVI216	994.1817	9.39047	105.8713	0
T2M_MAX16	60.66025	8.040807	7.544049	4.61E-14
Precip_cumsum16	0.642309	0.038645	16.62087	6.55E-62
(Intercept)17	3994.855	186.9733	21.36591	6.04E-101
GCVI217	1007.136	8.471123	118.8905	0
T2M_MAX17	-60.4923	6.621673	-9.1355	6.69E-20
Precip_cumsum17	0.666227	0.038186	17.44702	5.13E-68
(Intercept)18	10460.72	139.725	74.86652	0
GCVI218	1082.114	8.127424	133.1435	0
T2M_MAX18	-318.902	5.117332	-62.318	0
Precip_cumsum18	1.539709	0.039693	38.79053	0
(Intercept)19	5516.086	129.9902	42.43464	0
GCVI219	1053.252	8.290285	127.0465	0
T2M_MAX19	-128.085	4.737041	-27.039	3.76E-160
Precip_cumsum19	0.810469	0.038527	21.03655	6.31E-98
(Intercept)20	-8154.09	164.2641	-49.6401	0

GCVI220	1152.465	7.997403	144.1049	0
T2M_MAX20	324.7646	4.977024	65.25277	0
Precip_cumsum20	1.466977	0.039031	37.58478	6.00E-306
(Intercept)21	8230.678	131.5686	62.55805	0
GCVI221	932.0784	7.95548	117.1618	0
T2M_MAX21	-195.616	3.975056	-49.2108	0
Precip_cumsum21	0.826424	0.037528	22.02167	4.30E-107
(Intercept)22	16109.42	134.3429	119.9126	0
GCVI222	774.2819	7.54984	102.5561	0
T2M_MAX22	-452.622	4.159801	-108.809	0
Precip_cumsum22	2.245542	0.038277	58.66528	0
(Intercept)23	18777.09	153.9048	122.0045	0
GCVI223	711.7062	7.575187	93.9523	0
T2M_MAX23	-546.973	4.916533	-111.252	0
Precip_cumsum23	2.547111	0.038978	65.34658	0
(Intercept)24	16429.35	171.3886	95.86026	0
GCVI224	808.457	7.607446	106.2718	0
T2M_MAX24	-469.428	5.53172	-84.8612	0
Precip_cumsum24	1.830624	0.038678	47.32971	0
(Intercept)25	11438.57	152.9661	74.77847	0
GCVI225	806.0438	7.783914	103.5525	0
T2M_MAX25	-288.416	4.685946	-61.5492	0
Precip_cumsum25	0.923602	0.037075	24.91166	2.33E-136
(Intercept)26	11428.13	203.0016	56.29577	0
GCVI226	784.4962	8.010735	97.93061	0
T2M_MAX26	-268.258	6.000073	-44.7091	0
Precip_cumsum26	0.711828	0.037532	18.9658	5.31E-80
(Intercept)27	-751.152	144.1377	-5.21135	1.88E-07
GCVI227	927.3409	7.374364	125.752	0
T2M_MAX27	122.8366	5.003145	24.55188	1.60E-132
Precip_cumsum27	1.160119	0.040672	28.52378	6.95E-178
(Intercept)28	7666.621	176.3474	43.47454	0
GCVI228	816.8531	8.126792	100.5136	0
T2M_MAX28	-164.877	5.5277	-29.8275	3.24E-194
Precip_cumsum28	0.738762	0.037068	19.92982	4.05E-88
(Intercept)29	-2319.27	154.0124	-15.059	3.66E-51
GCVI229	1061.77	8.158729	130.1392	0
T2M_MAX29	152.9371	4.606905	33.19736	1.05E-239
Precip_cumsum29	0.979473	0.037963	25.80098	4.50E-146

(Intercept)30	9466.769	128.2866	73.79388	0
GCVI230	734.8154	7.780765	94.44	0
T2M_MAX30	-214.104	3.784562	-56.573	0
Precip_cumsum30	0.67326	0.035934	18.7362	3.98E-78
(Intercept)31	12348.16	119.3967	103.4212	0
GCVI231	674.9726	7.294503	92.53168	0
T2M_MAX31	-313.055	3.625156	-86.3562	0
Precip_cumsum31	1.163259	0.0353	32.95357	2.96E-236
(Intercept)32	15028.77	130.5159	115.149	0
GCVI232	715.3996	6.819731	104.9014	0
T2M_MAX32	-410.874	4.150269	-98.9993	0
Precip_cumsum32	1.365652	0.034932	39.09422	0
(Intercept)33	17465.82	168.2926	103.7825	0
GCVI233	658.7405	7.111468	92.63074	0
T2M_MAX33	-464.56	5.171724	-89.8269	0
Precip_cumsum33	0.928064	0.034784	26.68039	5.24E-156
(Intercept)34	5376.613	152.5221	35.25136	9.85E-270
GCVI234	855.6107	7.324159	116.8203	0
T2M_MAX34	-83.3351	4.81951	-17.2912	7.66E-67
Precip_cumsum34	0.686171	0.036643	18.72583	4.83E-78
(Intercept)35	1058.188	153.825	6.879166	6.07E-12
GCVI235	929.8213	7.439742	124.9803	0
T2M_MAX35	56.67518	4.595177	12.33362	6.52E-35
Precip_cumsum35	0.960209	0.040442	23.74302	4.24E-124
(Intercept)36	1684.211	160.0077	10.52581	6.88E-26
GCVI236	905.2751	7.020187	128.9531	0
T2M_MAX36	41.18678	5.098425	8.078333	6.67E-16
Precip_cumsum36	0.858131	0.03963	21.65342	1.28E-103
(Intercept)37	-8311.35	201.7029	-41.2059	0
GCVI237	920.7206	6.612934	139.2303	0
T2M_MAX37	396.9666	6.960961	57.02756	0
Precip_cumsum37	1.535221	0.038188	40.20195	0
(Intercept)38	1004.641	127.5472	7.876619	3.41E-15
GCVI238	885.9966	6.682929	132.5761	0
T2M_MAX38	77.2818	4.648946	16.62351	6.27E-62
Precip_cumsum38	0.64606	0.036065	17.91394	1.35E-71
(Intercept)39	-6328.3	125.8417	-50.2878	0
GCVI239	776.5988	6.582051	117.9874	0
T2M_MAX39	398.0082	5.10417	77.97705	0

Precip_cumsum39	1.136741	0.035293	32.20869	7.19E-226
(Intercept)40	2360.592	141.3033	16.70585	1.59E-62
GCVI240	892.9012	6.849082	130.368	0
T2M_MAX40	26.54448	5.521401	4.807561	1.53E-06
Precip_cumsum40	0.59858	0.036561	16.37221	3.96E-60
(Intercept)41	58.00319	121.724	0.476514	0.63371
GCVI241	896.5874	6.656795	134.6875	0
T2M_MAX41	106.9881	4.175256	25.62433	4.07E-144
Precip_cumsum41	0.702816	0.036228	19.40003	1.31E-83
(Intercept)42	9708.414	209.7558	46.28437	0
GCVI242	922.1937	6.649773	138.6805	0
T2M_MAX42	-245.502	7.540953	-32.5558	1.11E-230
Precip_cumsum42	0.674807	0.036015	18.73674	3.94E-78
(Intercept)43	11835.3	133.3508	88.75309	0
GCVI243	889.5668	6.475496	137.3743	0
T2M_MAX43	-314.122	4.526677	-69.3935	0
Precip_cumsum43	1.013172	0.035361	28.65258	1.82E-179
(Intercept)44	15370.42	129.9078	118.3179	0
GCVI244	738.9521	6.498735	113.7071	0
T2M_MAX44	-416.722	4.166825	-100.009	0
Precip_cumsum44	1.881194	0.035303	53.28759	0
(Intercept)45	16689.21	92.26753	180.8785	0
GCVI245	523.4395	6.221293	84.13676	0
T2M_MAX45	-437.059	2.720999	-160.624	0
Precip_cumsum45	2.725446	0.0328	83.09206	0
(Intercept)46	21280.99	123.6024	172.173	0
GCVI246	549.6549	6.265465	87.72771	0
T2M_MAX46	-591.144	3.820507	-154.729	0
Precip_cumsum46	1.853553	0.031602	58.65378	0
(Intercept)47	1784.758	161.2579	11.06772	1.90E-28
GCVI247	966.2993	7.178857	134.6035	0
T2M_MAX47	34.18807	4.881051	7.004245	2.51E-12
Precip_cumsum47	0.936648	0.039214	23.88527	1.47E-125
(Intercept)48	5719.489	112.1875	50.98153	0
GCVI248	898.2074	6.973944	128.7948	0
T2M_MAX48	-87.1789	3.237596	-26.9271	7.49E-159
Precip_cumsum48	0.703857	0.036077	19.50989	1.56E-84
(Intercept)49	11108.98	105.61	105.1887	0
GCVI249	836.2683	6.530213	128.0614	0

T2M_MAX49	-265.818	3.20461	-82.9487	0
Precip_cumsum49	0.902705	0.034265	26.3449	3.53E-152
(Intercept)50	14286.15	91.19407	156.6566	0
GCVI250	783.1077	6.085326	128.6879	0
T2M_MAX50	-389.48	2.890808	-134.731	0
Precip_cumsum50	2.538067	0.03433	73.93109	0
(Intercept)51	22488.43	135.5965	165.8482	0
GCVI251	1262.325	6.083523	207.499	0
T2M_MAX51	-799.468	5.371166	-148.844	0
Precip_cumsum51	3.799309	0.036982	102.7353	0
(Intercept)52	12079.03	88.40361	136.6351	0
GCVI252	1166.307	6.304929	184.9834	0
T2M_MAX52	-386.425	3.43438	-112.517	0
Precip_cumsum52	2.444736	0.03571	68.45993	0
(Intercept)53	10983.07	64.33661	170.7126	0
GCVI253	954.7859	5.769454	165.4898	0
T2M_MAX53	-325.479	2.244432	-145.016	0
Precip_cumsum53	2.631326	0.033261	79.11143	0
(Intercept)54	4969.563	126.337	39.33578	0
GCVI254	929.432	7.172479	129.5831	0
T2M_MAX54	-68.2407	4.054944	-16.829	2.02E-63
Precip_cumsum54	0.882928	0.036888	23.93515	4.48E-126
(Intercept)55	-4395.33	112.3567	-39.1194	0
GCVI255	1197.755	7.128355	168.0268	0
T2M_MAX55	231.6748	3.364754	68.8534	0
Precip_cumsum55	2.179933	0.03793	57.47245	0
(Intercept)56	-7556.64	94.13381	-80.2755	0
GCVI256	1291.251	6.531321	197.7013	0
T2M_MAX56	343.3249	2.88286	119.0918	0
Precip_cumsum56	3.015687	0.036064	83.62024	0
(Intercept)57	-6120.77	94.78474	-64.5755	0
GCVI257	1173.826	6.391085	183.6662	0
T2M_MAX57	320.1927	3.121508	102.5763	0
Precip_cumsum57	2.755639	0.036919	74.6407	0
(Intercept)58	7466.958	95.76755	77.96961	0
GCVI258	957.2591	6.486395	147.5795	0
T2M_MAX58	-165.865	3.300899	-50.2484	0
Precip_cumsum58	0.988592	0.034332	28.79474	3.21E-181
(Intercept)59	-3261.14	104.5606	-31.189	5.01E-212

GCVI259	952.9423	6.417623	148.4884	0
T2M_MAX59	261.7722	4.115316	63.60927	0
Precip_cumsum59	1.109264	0.033762	32.85546	7.12E-235
(Intercept)60	-1847.54	120.8112	-15.2928	1.05E-52
GCVI260	977.0856	6.532488	149.5733	0
T2M_MAX60	205.2127	4.880567	42.0469	0
Precip_cumsum60	0.631716	0.034553	18.28237	1.74E-74
(Intercept)61	2521.089	105.2385	23.95597	2.73E-126
GCVI261	1003.881	6.581387	152.5334	0
T2M_MAX61	21.33695	4.021611	5.305573	1.13E-07
Precip_cumsum61	0.888125	0.034933	25.42403	6.48E-142
(Intercept)62	2397.241	101.2733	23.67101	2.31E-123
GCVI262	1007.75	6.672743	151.0248	0
T2M_MAX62	25.62983	3.575212	7.168758	7.65E-13
Precip_cumsum62	0.918677	0.034817	26.38609	1.20E-152